A Honeycomb Proportional Counter for Photon Multiplicity Measurement in the ALICE Experiment

M.M.Aggarwal[1], S.K. Badyal[2], V.S. Bhatia[1], S. Chattopadhyay[3], A.K. Dubey[4], M.R. Dutta Majumdar[3], M.S. Ganti[3], P. Ghosh[3*], A. Kumar[1], T.K. Nayak[3], S. Mahajan[2], D.P. Mahapatra[4], L.K. Mangotra[2], B. Mohanty[4], S. Pal[3], S.C. Phatak[4], B.V.K.S. Potukuchi[2], R. Raniwala[5], S. Raniwala[5], N.K. Rao[2], R.N. Singaraju[3], Bikash Sinha[3], M.D. Trivedi[3], R.J. Veenhof[6], Y.P. Viyogi[3#]

[1]Physics Department, Panjab University, Chandigarh 160014, India; [2]Physics Department, Jammu University, Jammu 180001, India; [3]Variable Energy Cyclotron Centre, Calcutta 700064, India ; [4]Institute of Physics, Bhubaneswar 751005, India; [5]Physics Department, Rajasthan University, Jaipur 302004, India; [6]CERN, Geneva, Switzerland; *CSIR research fellow.

Abstract

A honeycomb detector consisting of a matrix of 96 closely packed hexagonal cells, each working as a proportional counter with a wire readout, was fabricated and tested at the CERN PS. The cell depth and the radial dimensions of the cell were small, in the range of 5-10 mm. The appropriate cell design was arrived at using GARFIELD simulations. Two geometries are described illustrating the effect of field shaping. The charged particle detection efficiency and the preshower characteristics have been studied using pion and electron beams. Average charged particle detection efficiency was found to be 98 %, which is almost uniform within the cell volume and also within the array. The preshower data show that the transverse size of the shower is in close agreement with the results of simulations for a range of energies and converter thicknesses.

#Corresponding author

Variable Energy Cyclotron Centre

Bidhan Nagar, Calcutta 700064 (India)

Tel. +91.33.3370032, Fax: +91.33.3346871

e-mail : viyogi@veccal.ernet.in

Keywords

Proportional counter, preshower detector, ALICE experiment, photon multiplicity detector

PACS : 24.85. +p; 25.75.-q

1 Introduction

The ALICE experiment is designed for a dedicated study of heavy ion collisions at the Large Hadron Collider at CERN, in order to study hadronic matter at high density and temperature and to probe the deconfinement transition and chiral symmetry restoration [1]. The design of the detector systems in ALICE has been based on the assumption that charged particle multiplicities in Pb + Pb collisions at a c.m. energy of 5.5 A.TeV could be as high as 8000 per unit rapidity at mid-rapidity, decreasing slowly at larger rapidities. In such a high multiplicity environment, a preshower Photon Multiplicity Detector (PMD) has been designed to measure photon multiplicities in the forward region and to provide estimates of transverse electromagnetic energy [2]. Using these measurements on an event by event basis, the PMD will be able to study event shapes and fluctuations [3, 4].

The basic principle of photon detection using the proposed PMD is similar to those of preshower detectors used in WA93 [5] and WA98 [6] experiments at the CERN SPS. It consists of a highly segmented detector placed behind a lead converter of suitable thickness. A photon produces an electromagnetic shower on passing through the converter. These shower particles produce signals in several cells of the sensitive volume of the detector. Charged hadrons usually affect only one cell and produce a signal resembling those of minimum ionizing particles (MIPs). The thickness of the converter is optimized such that the conversion probability of photons is high and the transverse shower spread is small to minimize shower overlap in a high multiplicity environment. A charged particle detector of similar granularity may be placed in front of the converter to act as veto in order to improve the discrimination between charged hadrons and photons.

The PMD will use gas as sensitive medium, as other options are either too expensive (e.g., scintillator readout) or not compatible with ALICE baseline detector (e.g., a silicon detector placed close to the vertex resulted in increased background into the Time Projection Chamber). The choice of detector technology for use in preshower applications is dictated by the consideration that (a) signal from charged particles is confined preferably to one cell, and (b) low energy δ-electrons should be prevented from traveling to nearby cells and causing cross-talk among adjacent channels.

The conventional technology of gas detectors employs a large uniform gas volume with

cathode pad readout. In these detectors a single charged particle invariably affects more than one pad owing to the capacitive coupling between them or due to δ-electrons traveling at large angles. This leads to spreading of the signals to regions much beyond the actual shower region.

Segmentation of the gas volume with material separation thus becomes necessary to reduce the effect of δ-electrons. Some attempts have been made in the past to develop such segmented proportional chambers [7, 8]. However, they do not suit our requirements of small gas thickness, field homogeneity and material thickness.

We have used a honeycomb cellular geometry for segmentation and field shaping. Several prototypes of the PMD have been fabricated. These have been tested at CERN using pion and electron beams at various energies [2, 9]. The same design will also be used for the PMD in the STAR experiment at RHIC [10]. In this article we present an account of the design, fabrication and the performance of these prototypes. Section 2 describes the detector design and the cell modeling. In section 3 we describe the fabrication procedure of the honeycomb prototype. The test data are discussed in detail in section 4. A summary is presented in section 5.

2 Design considerations and cell modeling

The most important requirement for the present detector, apart from high efficiency for charged particle detection, is that the signals from charged hadrons be confined to one cell. This will help to minimize the occupancy in both preshower and veto applications. In addition, the design is also influenced by the following considerations for a preshower detector :

- the active volume of the detector should be thin and very close to the converter so that the transverse spread of the shower is minimized,
- low-energy δ-electrons should be prevented from traveling to nearby cells, in order to minimize crosstalk among adjacent channels,
- the technology should be amenable to modular design with a minimum of dead space at the boundaries and should not require a staggered layout,

- the detector material (gas) should be insensitive to neutrons. In a hydrogeneous medium neutrons tend to produce large signals due to recoil protons, which can mimic a photon signal.

Based on the above considerations a honeycomb chamber design was adopted. The honeycomb body made up of copper forms the common cathode and is kept at large negative potential. The anode wire is kept at ground potential, which facilitates easy coupling with front-end electronics. The cells are thus physically isolated from each other by copper walls of suitable thickness to contain the δ-electrons. Optimum values of cell depth and copper wall thickness have been obtained from GEANT simulation [11] of preshower development in such a detector.

In a normal proportional chamber the aspect ratio (ratio of cell radius and wire length) is generally very small. In the present case smaller cell depth (around 10 mm) and comparable cell diameter makes the aspect ratio relatively large. This design makes our detector an unconventional one, where the edge effects at the wire ends dominate. The end effects have a direct bearing on the efficiency of charge particle detection. Hence proper field shaping had to be done to minimize these end effects [2]. Appropriate cell configuration has been arrived at by cell modeling and prototype tests.

A schematic diagram of the hexagonal unit cell and its cross section are shown in Fig. 1. The cell volume is sealed by FR4 printed circuit boards (PCBs, referred to as 'lids' in the figure). The cell simulations were carried out using MAXWELL [12] and GARFIELD [13] software packages. The detector cell is modeled in MAXWELL according to the parameters given in Table 1. Because of the six fold axial symmetry of the cell and a mirror symmetry in the plane perpendicular to the tube axis, only 1/12 of the whole cell was modeled in MAXWELL. The field maps for the entire cell were then generated by GARFIELD using these symmetry considerations.

Two geometries of the cathode have been studied as shown in Fig. 1. For the cell shown in Fig. 1(b), the cathode resembles an open tubular structure. This is referred to as open geometry cell. In Fig. 1(c) the cathode of the cell is extended close to the anode wire. This 'extended cathode cell' will be described later.

The field configuration within the cell is studied with the help of drift line plots for the two geometries. An electron drift-line plot is shown for the open geometry cell in Fig. 2 for two tracks at different distances from the anode wire. For tracks a little far away from the wire, a large fraction of these electrons do not reach the wire and escape the drift medium, as shown by dashed lines in the figure. The loss in the collection of the primary electrons increases as the distance from the anode wire increases. This affects the efficiency of charged particle detection. The problem becomes acute in the present case where smaller gas depth limits the primary ionization.

The charge collection on the anode can be improved with proper field shaping. Guard rings have been traditionally used for field shaping in gas counters. However fabrication and optimization of guard rings becomes difficult for large arrays with segmented cells. As a simple alternative, the cathode was extended on the inner copper surface of the lids (using double sided PCBs) up to 2 mm from the wire. This is shown schematically in Fig. 1(c). This cell is referred to as extended cathode cell. The thickness of the extended portion of the cathode was taken as 50 μm for GARFIELD simulations.

The electron drift-line plot for the extended cathode cell is shown in Fig. 3. It shows that the electrons generated almost anywhere inside the volume reach the anode. Only for a small portion of the region on either ends, some electrons still escape the drift medium and hit the lids, as shown by dashed lines. But this region amounts to less than about 10 % of the entire volume. This suggests that the extended cathode design should have better uniformity of response within a cell.

3 Prototype fabrication

The construction of the honeycomb prototype involved two main steps – fabrication of the honeycomb matrix and assembly of the chamber.

Copper strips of thickness 0.2 mm with small notches cut at regular intervals on both edges were shaped in the form of a half-honeycomb using a precision-machined hexagonal jig. The width of the strip, varying from 8 mm to 12 mm, determined the gas thickness of the detector. Joining two such half-honeycomb strips by spot-soldering resulted in a row of hexagonal cells. In this scheme four sides of the hexagon had a thickness equal to the

original thickness of the strip and two sides had double the thickness. In the final shape notches appeared on all sides of the hexagonal cells. This facilitated smooth gas flow within all cells in the chamber. The honeycomb matrix was then cleaned with a soap solution and coated with graphite paint to improve the aging properties and to suppress after-pulsing. A FR4 frame was machined to house the honeycomb. Gas flow nozzles were fitted on the sides of the frame. A photograph of the components of the chamber is shown in Fig. 4.

The honeycomb matrix was sandwiched between two printed circuit boards (PCBs), each of thickness 1.5 mm. One side of these PCBs had solder islands (1 mm $\times$ 4 mm) at the center of each cell and thin (0.25 mm) tracks leading to 50-pin connectors. While one board contained the full wiring layout of the tracks, the other had only solder islands to anchor the anode wires. One PCB was first bonded with epoxy to the FR4 frame. The edges of the honeycomb were glued to it after checking the alignment. The second PCB was then bonded to the other side of the frame, taking care of the hole alignment and proper connection of the cathode (honeycomb) to the SHV connector. For the extended cathode prototypes, the inner surface of the PCBs consisted of tin-plated copper layer in contact with the honeycomb cathode, and annular gaps of insulated rings of 2 mm radius around the ends of the central anode wire.

Gold plated tungsten wire (20 μm in diameter), after proper cleaning, was inserted through the holes of the PCB using a wire insertion jig. The jig consisted of a small plastic wire spool on an aluminum frame with hypodermic syringe needle fitted to the frame. The wire was drawn through the capillary of the needle and inserted through the PCB holes together with the needle. The needle was withdrawn after soldering the wire on to the rear PCB. The wire was stretched to a tension of 25 g (equivalent to 30% of its elastic limit) using a spring loaded slider on the spool, before being soldered on to the front PCBs. Care was taken while soldering to prevent flux creepage into the cell. The holes were then closed by high viscosity fast-setting epoxy. Two thin copper-clad printed boards were again bonded on the soldered surface of the above mentioned PCBs, with copper on the outer surface to make a proper shielding for the entire readout connections. The details can be found in Ref [2].

Negative high voltage was applied to the honeycomb cathode through a high value (2.2 MΩ) non inductive resistor with a high voltage decoupling capacitor. The readout boards

containing front-end electronics were connected on the chamber as shown in Fig. 4.

4 Test setup, analysis and results

We describe the results for three prototypes of different geometrical configurations as given in Table 2.

4.1 The test beam setup

The prototype chamber was tested at the T10 beam-line of the CERN Proton Synchrotron. The response of the detector to charged particles was studied using 7 GeV/c pion beams. The test setup consisted of three pairs of cathode strip chambers (CSC) with the prototype detector placed in between the last two CSCs as shown in the Fig. 5 (a). The CSCs were used for tracking the pion beams. Two pairs of crossed scintillators in a 4-fold coincidence provided the charged particle trigger.

The setup for preshower studies is schematically shown in Fig. 5 (b). A lead converter of suitable thickness was kept just in front of the honeycomb chamber. A gas based Cerenkov detector was used to provide the electron trigger in coincidence with the two pairs of the scintillators.

The prototype chamber was mounted on a stand having horizontal and vertical movements, reproducible to within a millimeter, facilitating the study of the response of individual cells in the detector. The pair of trigger scintillators had an overlap of about 1 cm^2 which was comparable to the area of each hexagonal cell. Hence for most of the studies related to the detector response, the chamber could be positioned in such a way that the beam profile was confined to almost one cell. A steady flow of Ar-CO_2 gas mixture was maintained in the prototype honeycomb detector.

The readout of the prototype chamber was carried out using GASSIPLEX electronics (1.5 μm version) [14] and a C-RAMS based data acquisition setup [15]. For the prototype detector in the present case, which generates negative pulses, the dynamic range of GASSIPLEX was 75 fC and the output pulse was limited to -1V. The pedestal was around 160 ADC channels. The r.m.s deviation of the pedestal, which is a measure of the noise in the

system, was ∼1.5 units.

4.2 Tracking and clustering

Tracking was done with the help of CSCs. These provided an external reference for the impact point of the particle on the prototype chamber. In all cases only single-hit tracks having good reconstruction in all the 6 planes were taken. A straight line was fit by least square method by taking the centroids of the clusters for every track in the 3 pairs of CSC's. Accordingly the impact point for every track was projected in the plane of the prototype detector. These projected coordinates were then used to form 2 mm bins to study the variation in the efficiency within the cell.

Particles entering the chamber can at times affect more than one cell. Hence the cell hits were first clustered using a nearest neighbour clustering algorithm. For every hit cell, two concentric rings comprising of 19 cells were scanned to identify contiguous cells which might have been affected. The ADC channel contents in all the cells falling within the cluster were added together to represent the pulse height corresponding to the total energy deposited by the incident particle.

4.3 Characteristics of charged particle detection

Typical pulse height spectra for two prototypes (having cell depths respectively 10 mm and 8 mm) are shown in Fig. 6(a) along with a fit to a Landau distribution. The detectors were operated at -1520 V and -1450 V respectively. The operating gas in both the cases was a mixture of Ar and CO_2 (in the ratio 70:30 by weight). The mean value of the pulse height spectra is taken as the measure of the average energy deposited by the charged particle. The distribution of the cluster size (number of cells fired) for charged particles for the above operating conditions of the detector is shown in Fig. 6 (b). The average cluster size is close to unity, suggesting that the energy deposition is essentially confined to one cell. This satisfies one of the basic design criteria of our detector.

4.3.1 Optimization of operating conditions

The operating conditions for the detector refer to appropriate detector bias voltage and the gas mixture. These were optimized after a detailed study of variation of the charged particle detection efficiency in the proportional region.

Fig 7 (a) shows the variation of efficiency with voltage for different gas mixtures using extended cathode prototypes of 8 mm gas thickness (prototype-99-8) and 10 mm prototype (prototype-99-10). We observe that the efficiency increases with voltage and at about -1450 Volts, it reaches a plateau region. The variation of the peak pulse height with the applied voltage is shown in Fig 7(b) for a given gas mixture and cell geometry. We observe that around the same voltage of -1450 Volts the peak pulse height varies almost linearly with voltage indicating the onset of the proportional region.

A higher percentage of Ar in the gas mixture increases the detection efficiency of charged particles, but the longer tails in the signal are removed faster if the percentage of CO_2 is higher, which is important for handling a higher rate of particle fluxes [16]. In the present study with a gas mixture of Ar and CO_2 in the ratio 70 : 30, stable operation of the detector was achieved with efficiency comparable to those with higher percentage of Argon. This suggests that the detector may be able to handle high count rates without loss of detection efficiency. Final optimization of the gas mixture will be done after a study of the count rate behaviour.

4.3.2 Variation of efficiency and pulse height within the cell

A high statistics scan of the chamber was taken for selected cells to study the variation of efficiency within the cell in smaller bins in horizontal and vertical directions. Tracking was done using the hits on the CSCs to get the projected hits on the detector plane. These hits were analyzed for sliding square bins of 2 mm width and 2 mm height. Fig. 8 shows the variation of this efficiency with horizontal position (scanned across three cells) for both open geometry and extended cathode cells. It shows a flat region in the central part of the cell, indicating the uniformity in efficiency. Compared to open geometry cells, the extended cathode cells give much flatter efficiency as a function of position along the cross-section of the cell.

At the edges, while the efficiency drops to 70 % in case of the open geometry cell, it is above 90 % for the extended cathode geometry. The large drop in efficiency for the open geometry cell at the edges is due to the poor charge collection for tracks at the edges, as observed from the drift line plots for this geometry (see Fig. 2). The distance between the consecutive dips reflects the cell wall separation for both cell geometries.

We have also studied the variation of pulse height as a function of the radial distance of the beam tracks. Fig. 9 shows the peak pulse height for tracks at varying radial distances from the wire. The GARFIELD simulation results, without the effect of electronics, are shown by a solid line. The simulation results describe the observed behaviour reasonably well. Considering that the r.m.s. deviation of pedestals was $\sim$1.5 units, a noise threshold of 6 ADC channels (corresponding to 4σ values) was applied to the pulse height data during analysis. The plot clearly shows that the peak pulse height is greater than the noise threshold by a factor of 5 or more, for tracks at all distances from the wire. This suggests that for the present detector and electronics system, the signal to noise ratio for minimum ionizing particles is better than 5:1.

4.3.3 Cell-to-cell variation of efficiency and average pulse height

About 40 cells in the prototype were randomly selected and the beam positioned in the center of each cell to study the charged particle detection efficiency and average pulse height. The relative gains of the cells defined by the ratio of the mean pulse height in a cell to the average value of the mean pulse heights of all the 40 cells taken together is shown in the Fig 10. The overall gain of the prototype chamber was found to be quite uniform, the distribution having a narrow width of $\sigma \sim 6\%$. The mean efficiency of the different cells scanned for the prototype with extended cathode and 8 mm cell depth was found to be $\sim 98\%$ as shown in the Fig 10. The average efficiency for the prototype with extended cathode and 10 mm cell depth was also close to the above value.

4.4 Preshower characteristics

The preshower characteristics were studied for the extended cathode prototype-99-8 detector using electron beams in the energy range of 1–6 GeV at two different operating voltages using

2 X_0 and 3 X_0 converter thicknesses. The results are described below.

4.4.1 Transverse shower spread

The electron beam passing through the lead converter produces an electromagnetic shower and thus affects several cells in the detector. The average number of cells affected gives us an estimate of the transverse shower size.

A typical distribution of the preshower cluster size (number of cells affected) for 3 GeV electrons with a 3 X_0 thick converter is shown in Fig. 11.

The preshower cluster size has been studied for several combinations of electron energies and converter thicknesses. The results are summarized in Fig. 12. Comparing the results with the single particle GEANT simulation for electrons, it was found that the average preshower cluster size is very close to that obtained in simulation. This is a very important result and represents a marked improvement over the WA98 PMD case where the preshower cluster size in test data was about twice that obtained in simulation [6]. The present results suggest that the final occupancy in the actual experiment will be close to those obtained in GEANT simulations.

4.4.2 Energy deposition spectra in a preshower

Total energy deposition in a preshower is represented by the sum of signals (ADC contents) of all the affected cells in a cluster. Pulse height spectra representing energy deposition for different electron energies for a 3 X_0 thick converter are shown in Fig 13. The left panels show the test data and the right panels show the simulation results. The two sets of spectra look similar in shape. The average energy deposition increases with increasing electron energy. The relative widths in the preshower spectra are larger than those in simulation. This is due to fluctuations in gas ionization, signal generation and transmission processes in data, which are not accounted for in GEANT simulation.

4.4.3 Energy – ADC calibration relation

A comparison of test data with simulation allows us to understand the features specific to the readout system and cross-talks, if any, and to parameterize the effects. In view of this, the mean pulse height in ADC units as obtained from data is plotted against the mean energy deposition values in keV from the simulation spectra for different electron energies and converter thicknesses. Fig. 14 shows the calibration relation for an operating voltage of -1465 V. The response of the detector and readout is seen to be fairly linear in the range of energy studied. The present study extends to average energy deposition of ∼60 keV, which corresponds to the energy deposited by 10 GeV photons in the preshower part of the PMD.

5 Summary

In the present article, we have described the design, simulation and the test data of a gas based honeycomb proportional counter for photon multiplicity measurements in the ALICE experiment. The design is based on a copper honeycomb matrix as cathode and anode wires placed at the center of each cell. The detector is operated using Ar–CO_2 gas mixture with the cathode at a high negative potential, and the anode wire at ground potential. The diameter of the cell and the depth (length of the wire) are comparable, being in the range of 8-10 mm. Two geometries of the cell, with different cathode structures, have been studied. The design has been optimized by GARFIELD simulations and by prototype studies using high energy pion and electron beams.

The cellular design is found to contain δ-electrons and minimize the spread of the signal to neighbouring cells. The charged particle signal is confined mostly to one cell. This satisfies one of the basic requirements of our design. Operating conditions like the cathode voltage and the proportion of Ar and CO_2 in the gas mixture have been optimized by prototype tests. The efficiency for open geometry cell drops considerably near the edges of the hexagon, but for the extended cathode cells, it is quite uniform throughout the volume of the cell. With the extended cathode prototype of 8 mm gas thickness, under an optimized condition of gas mixture and operating voltage, the average charged particle detection efficiency was found to be ∼98%. A study of a large number of cells of the extended cathode variety shows that the relative gains and detection efficiencies remain almost uniform throughout the detector,

cell-to-cell relative gain varying within 6%.

The preshower data show that the transverse shower size is in close agreement with single particle GEANT simulations for a range of converter thicknesses and electron energies. Average pulse height of the preshower follows a linear relation with energy deposition for a wide range, upto that expected from 10 GeV photons in the preshower part of the ALICE PMD.

Acknowledgements

We wish to express our gratitude to the accelerator crew for the excellent performance of the PS at CERN. We acknowledge the help of S. Iranzo and T. Lopez for help in running the MAXWELL code. We are thankful to H. Gutbrod, P. Martinengo, A. di Mauro, G. Paic, F. Piuz, J.C. Santiard, J. Schukraft and P. Szymanski for many useful suggestions and help during tests. We gratefully acknowledge the financial support of the Department of Atomic Energy, the Department of Science and Technology of the Government of India and the CERN PPE Division for this project. One of us (PG) acknowledges the grant of research fellowship of the Council of Scientific and Industrial Research in India.

References

[1] ALICE Collaboration, Technical Proposal, CERN/LHCC/ 95-71 (1995).

[2] ALICE Collaboration, Technical Design Report for PMD, CERN/LHCC/99-32 (1999).

[3] M.M. Aggarwal et al., WA93 Collaboration, Phys. Lett. B403 (1997) 390.

[4] M.M. Aggarwal et al., WA98 Collaboration, Phys. Rev. C64 (2001) 011901R and nucl-ex/0108029.

[5] M.M. Aggarwal et al., Nucl. Instr. Meth. in Phys. Res. A372 (1996) 143.

[6] M.M. Aggarwal et al., Nucl. Instr. Meth. in Phys. Res. A424 (1999) 395.

[7] V. Balagura, Nucl. Instr. Meth. in Phys. Res. A368 (1995) 252.

[8] R.T. Jones et al., Nucl. Instr. Meth. in Phys. Res. A343 (1994) 208.

[9] A.K. Dubey et al., ALICE Internal Note 99-16 (1999).

[10] D.P. Mahapatra et al., STAR Note SN-310 (1997).

[11] R. Brun et al., GEANT3 users' guide, CERN/DD/EE/84-1, R. Brun et al., CERN program library, W5013.

[12] Maxwell 3D Field Simulator version 4.1, Ansoft Corporation, USA, supported at CERN.

[13] R. Veenhof, CERN Programme Library, entry W5050;
Igor Smirnov, Heed: simulation of ionization losses in gas mixtures, version 1.01 (1996);
Stephen Biagi, Magboltz: calculation of transport properties in gas mixtures, version 1 (1997);
Rob Veenhof, Garfield: simulation of gaseous detectors, version 6.26 (1999).

[14] J.-C. Santiard et al., CERN-ECP/94-17; J.-C. Santiard et al., CERN/LHCC/96-39.

[15] ALICE Collaboration Technical Design Report for HMPID, CERN/LHCC 98-15 (1998).

[16] F. Sauli, CERN-77-09, May 1977; also F. Sauli in "Experimental Techniques In High Energy Nuclear and Particle Physics", ed. T. Ferbal, second edition, World Scientific, 1991.

Table 1: Parameters of the unit cell for simulation

Cell radius (typical)	6 mm
Cell depth/Wire length (typical)	8 mm
Radius of anode wire	10 microns
Thickness of inner FR4 plates (the 'lids')	1.5 mm
Thickness of the outer FR4 plates	1.2 mm
Gap between two FR4 plates	1.2 mm
Dielectric constant of FR4	4.4
Thickness of cell wall	0.2 mm
Cathode potential	-1400 V

Table 2: Geometrical parameters of the prototypes tested.

Cell cross-section	Cell depth	Cathode design	Reference in text
130 sq.mm.	12 mm	Open geometry	prototype-98
100 sq.mm.	10 mm	Extended cathode	prototype-99-10
100 sq.mm.	8 mm	Extended cathode	prototype-99-8

Figure Captions

1. (a) Schematic of a hexagonal cell with coordinate representations following GARFIELD convention. (b) Cross-section of the cell in xz-plane with dimensions used in GARFIELD simulations. The cathode is limited to the cell wall. This is referred as 'open geometry cell'. (c) Section showing the modified cathode design, extended on the inner face of the lids and brought close to the anode wire. The cell with this shape is referred as 'extended cathode cell'.

2. Electron drift lines inside the cell volume in xz-plane for an open geometry cell. The thick line in the center represents the anode wire. Drift lines for a track 3 mm away from the anode are shown on the lower part of the figure and those for a track 5 mm from the anode are shown in the upper part. Dashed lines represent drift lines escaping

the drift medium and falling on the body of the cell.

3. Electron drift lines inside the cell volume in xz-plane for an extended cathode cell. The thick line in the center represented anode wire. Dashed lines represent drift lines escaping the drift medium and falling on the body of the cell.

4. Components of a prototype honeycomb proportional counter showing the honeycomb array, the PCBs and the GASSIPLEX board. In the assembled version, the PCBs form part of a gas-tight chamber having a high voltage connection and inlet/outlet for the gas. The gas inlet is visible in the picture.

5. Schematic of the test beam arrangement. (a) setup for pion trigger, (b) setup for preshower studies with a lead converter (shown as dark block) in front of the honeycomb detector (PMD) and a Cerenkov counter for electron trigger.

6. Response of the extended cathode prototype to a 7 GeV pion beam. Left part : pulse height spectra for the two prototypes along with fits using the Landau distribution shown by solid lines. Operating voltages are shown in the figure. Right: Distribution of cluster size for pions passing through prototype-99-8.

7. (a) Variation in the efficiency of charged particle detection with applied voltage for different prototypes and gas mixtures, (b) Variation of the peak pulse height (ADC) as a function of applied voltage for the prototype-99-8.

8. Variation of efficiency with position within a cell for three different prototypes of open geometry and extended cathode cells. The figure shows a scan of three cells encompassing both sides of the boundaries of the central cell.

9. Variation of the peak pulse height with radius r for the extended cathode cells (prototype-99-8) along with GARFIELD simulation results.

10. (a) Relative gains of various cells in prototype-99-8 extended cathode geometry, and (b) efficiencies of the cells.

11. Distribution of cluster size for a typical preshower of 3 GeV electrons passing through a 3 X_0 thick lead converter.

12. Average cluster size for electron preshower at different energies. The operating voltages and the converter thicknesses used are shown in the figure. The filled circles denote test data and the open circles are GEANT simulation results.

13. Preshower spectra for different electron energies for a 3 X_0 converter thickness. The left panel shows the test data while the right panel shows simulation results.

14. Average cluster signal (ADC) vs. energy deposition for various combinations of electron energy and converter thickness used in the preshower studies at 1465 V.

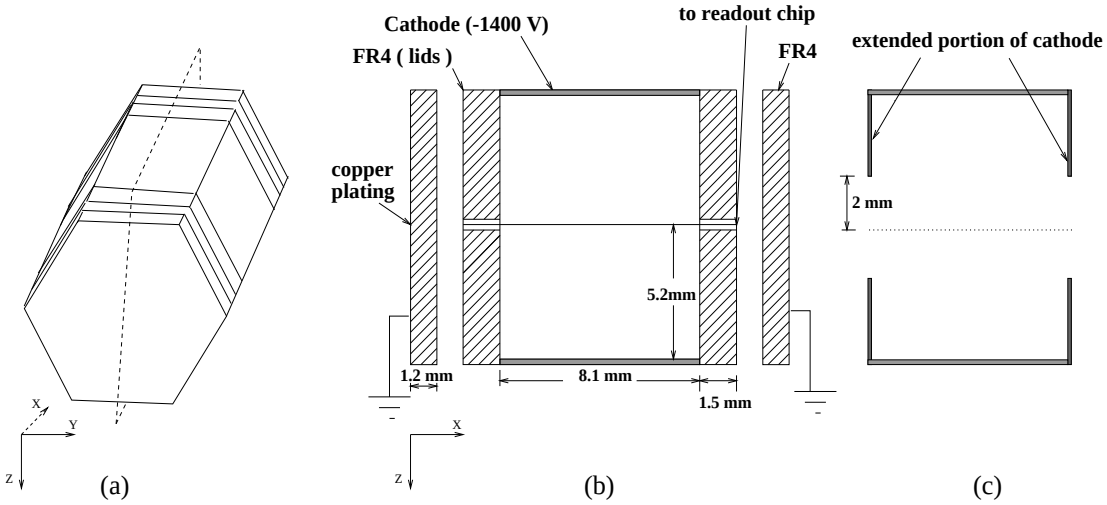

Figure 1:

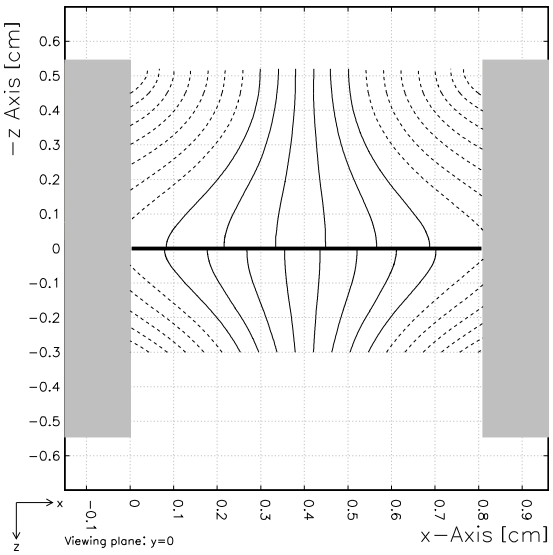

Figure 2:

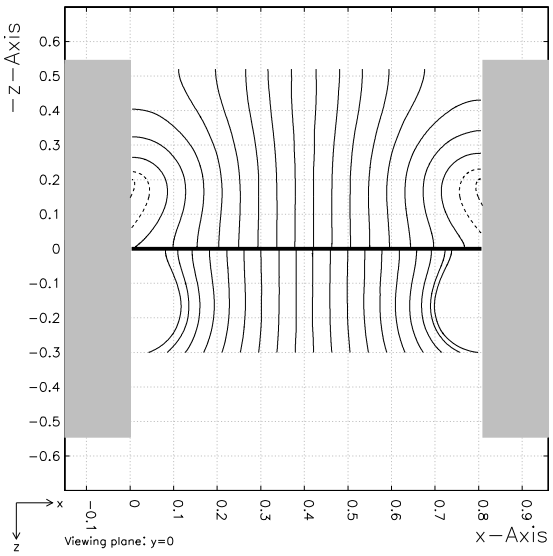

Figure 3:

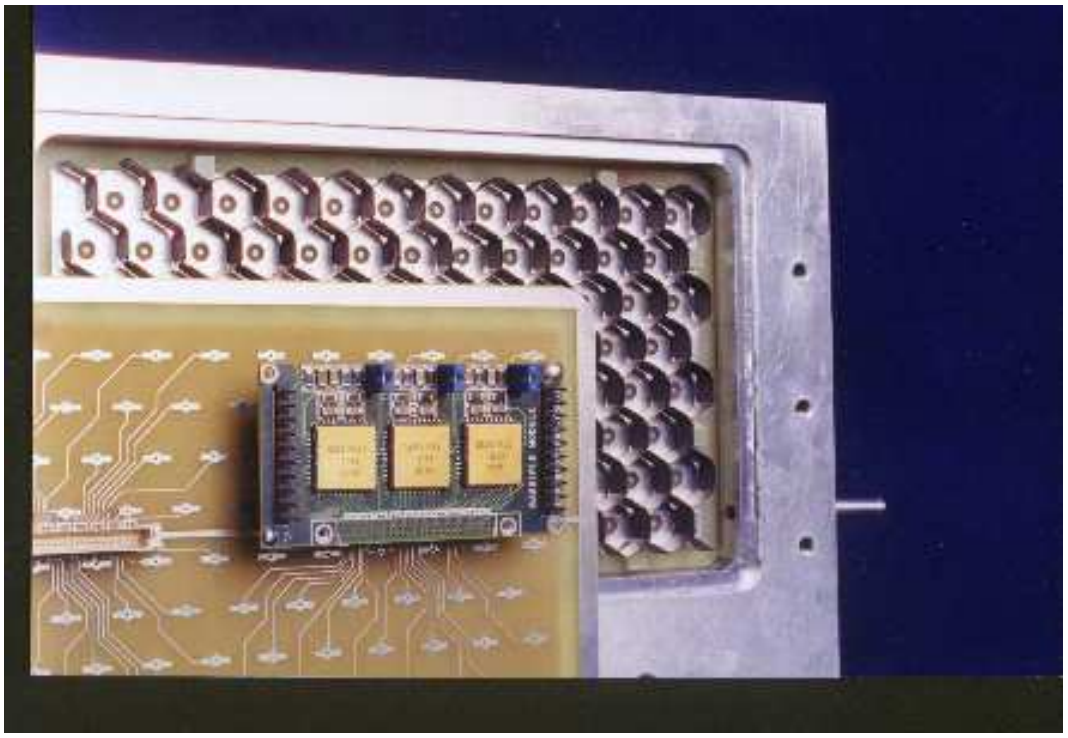

Figure 4:

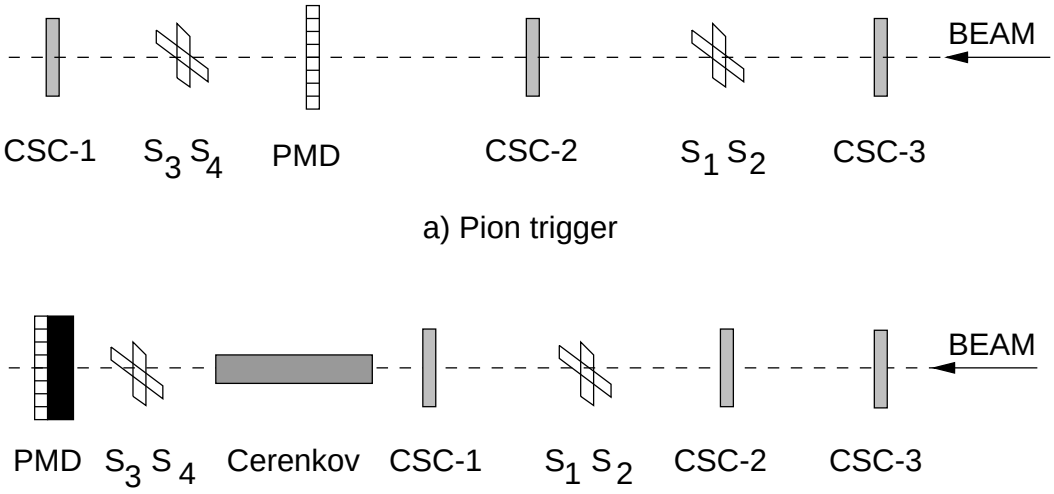

Figure 5:

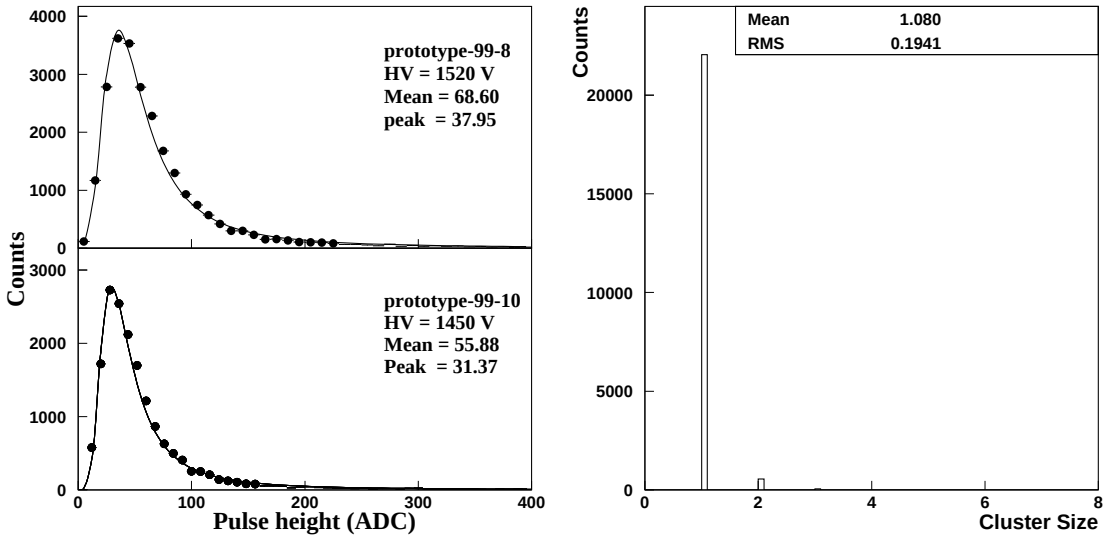

Figure 6:

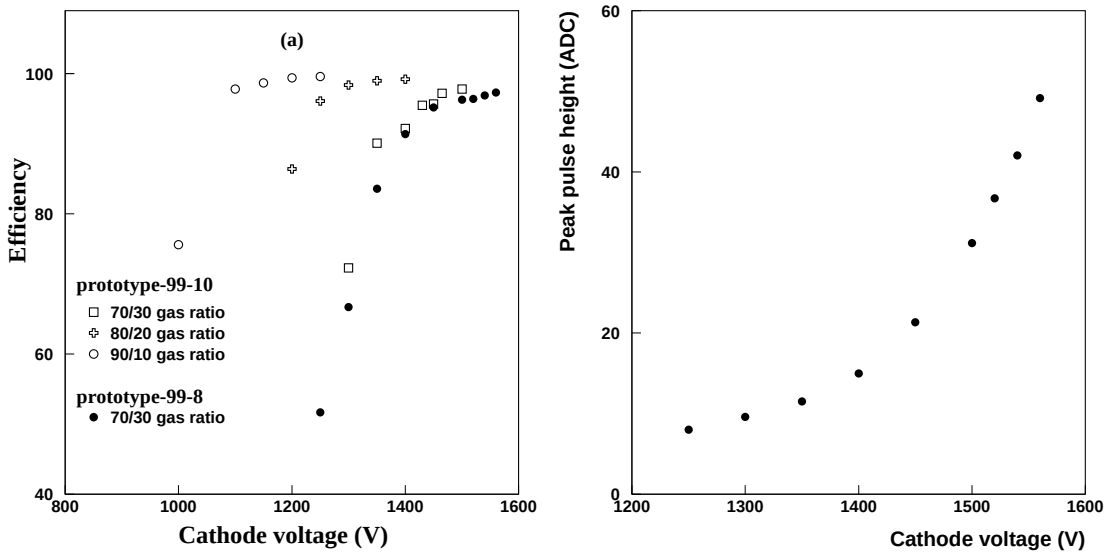

Figure 7:

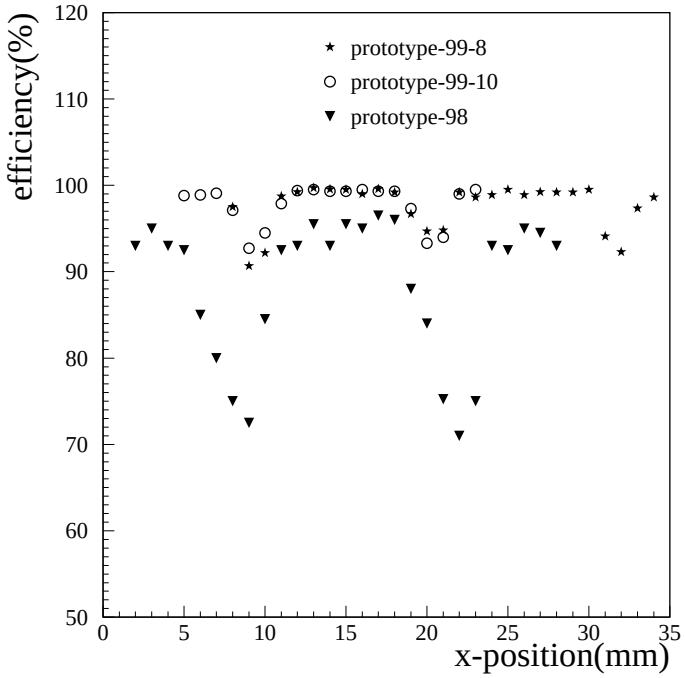

Figure 8:

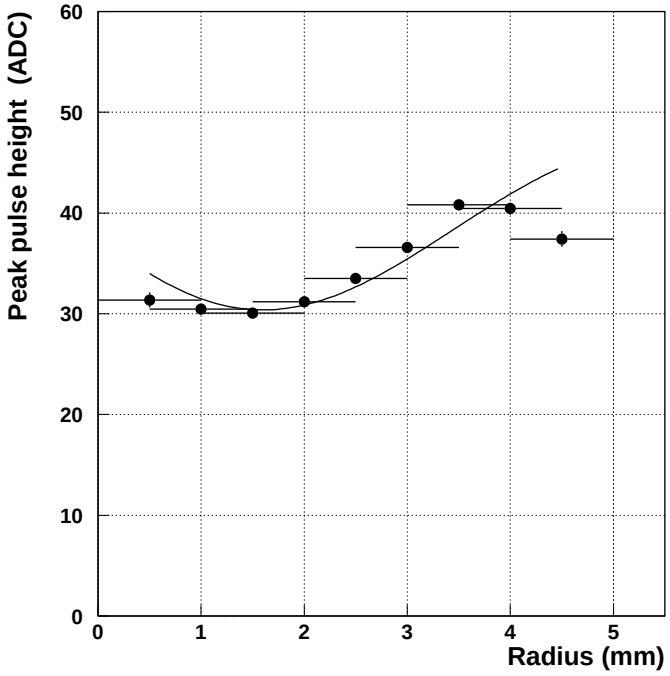

Figure 9:

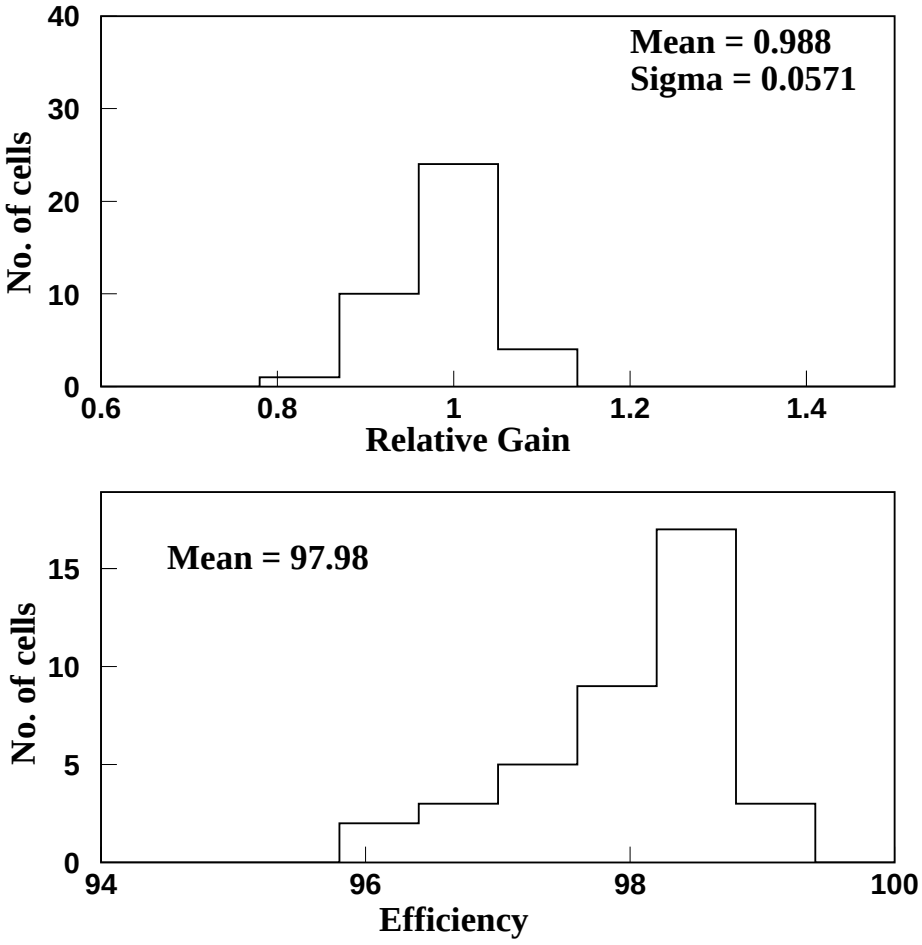
Mean = 0.988
Sigma = 0.0571
No. of cells
Relative Gain
Mean = 97.98
No. of cells
Efficiency

Figure 10:

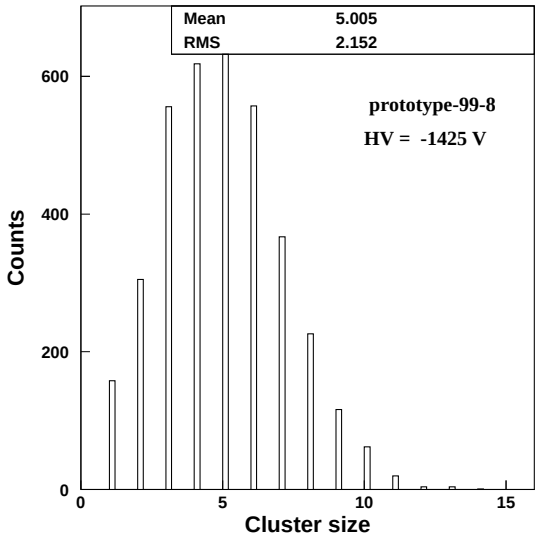

Figure 11:

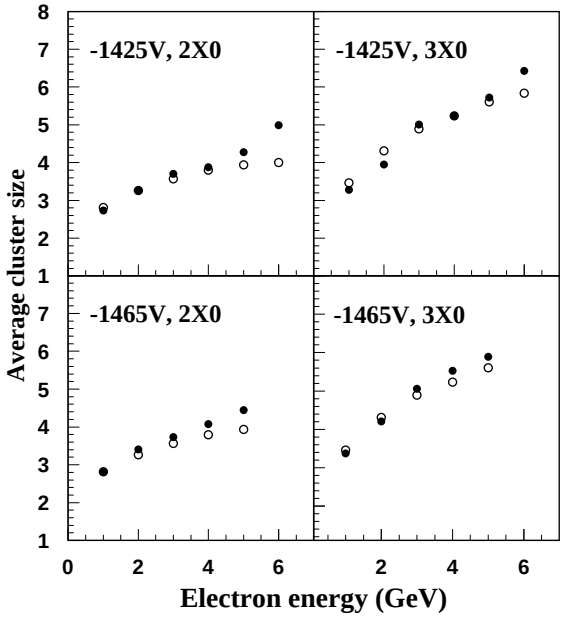

Figure 12:

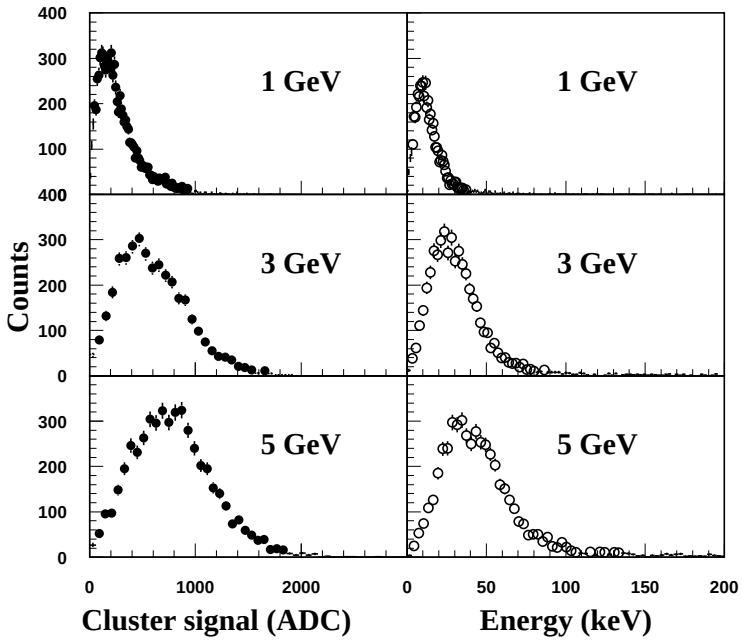
Counts
1 GeV
1 GeV
3 GeV
3 GeV
5 GeV
5 GeV
Cluster signal (ADC)
Energy (keV)

Figure 13:

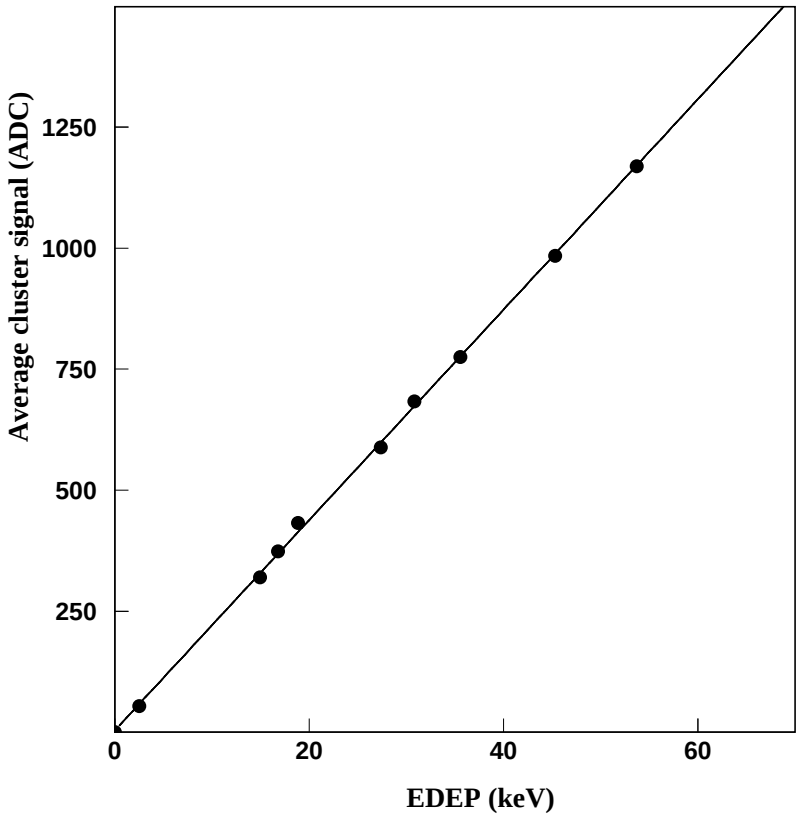
Average cluster signal (ADC)
1250
1000
750
500
250
0
20
40
60
EDEP (keV)

Figure 14: